Supporting Information for "Inversion of Longer-Period OBS Waveforms for P Structures in the Oceanic Lithosphere and Asthenosphere"

Nozomu Takeuchi,[1] Hitoshi Kawakatsu[1] Hajime Shiobara,[1] Takehi Isse,[1]

Hiroko Sugioka,[2] Aki Ito,[3] and Hisashi Utada[1]

Contents of this file

1. Text S1 to S2
2. Figures S1 to S15
3. Table S1

---

[1]Earthquake Research Institute,

University of Tokyo, Bunkyo-ku, Tokyo,

JAPAN.

[2]Graduate School of Science, Kobe

University, Kobe, Hyogo, JAPAN.

[3]Research Institute for Marine

Geodynamics, Japan Agency for

Marine-Earth Science and Technology,

Yokosuka, Kanagawa, JAPAN.

Introduction This supporting information provides additional information for the method used and results obtained in the main text.

Text S1. The velocity surfaces assumed in Section 3.1 are illustrated in Fig. S1. For each azimuth, ϕ, and incident angle, θ, we appropriately extrapolated the P and S velocities. We assumed that the S velocity surface is always circular. We assumed that the P velocity surface is always elliptic (or satisfies the elliptic condition). The isotropic part of the P velocity V_P and the vertical P velocity α_v are equal to the average horizontal velocity (α_h averaged over ϕ).

Text S2. Data bins were defined according to the event and array pairs such that the data in each bin sample similar regions with similar azimuths (Fig. S2). The pairs between the Area-A array and the events at the longitudes of $34^\circ - 42^\circ$N are categorized as Data Bin 1. The pairs between the Area-A and Area-B arrays and the events at $42^\circ-$N are categorized as Data Bin 2. Except for the 5 traces for the event in the Izu-Bonin region, all of the datasets whose distances are less than 15° are categorized into either Data Bin 1 or Data Bin 2.

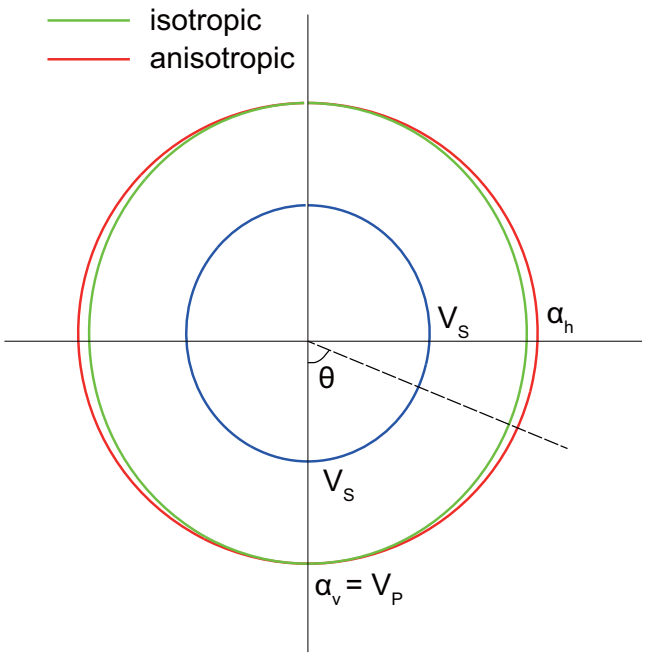

Figure S1. Assumed velocity surface (i.e., dependence of the incident angle, θ) for a specific azimuth, ϕ. V_P and V_s are the isotropic part of the P and S velocities, respectively, while α_h and α_v are the horizontal and vertical P velocities, respectively.

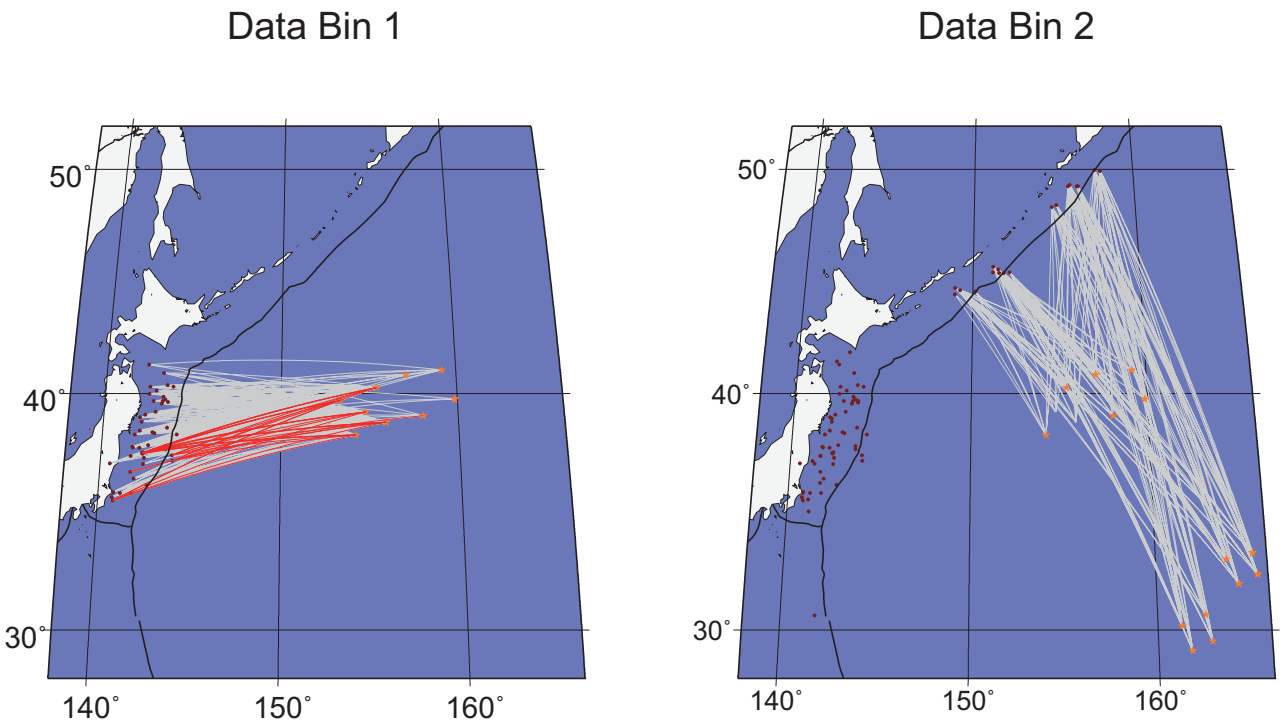

Figure S2. Definitions of Data Bin 1 and Data Bin 2. The anomalous waveforms in Data Bin 1 are denoted by the red lines.

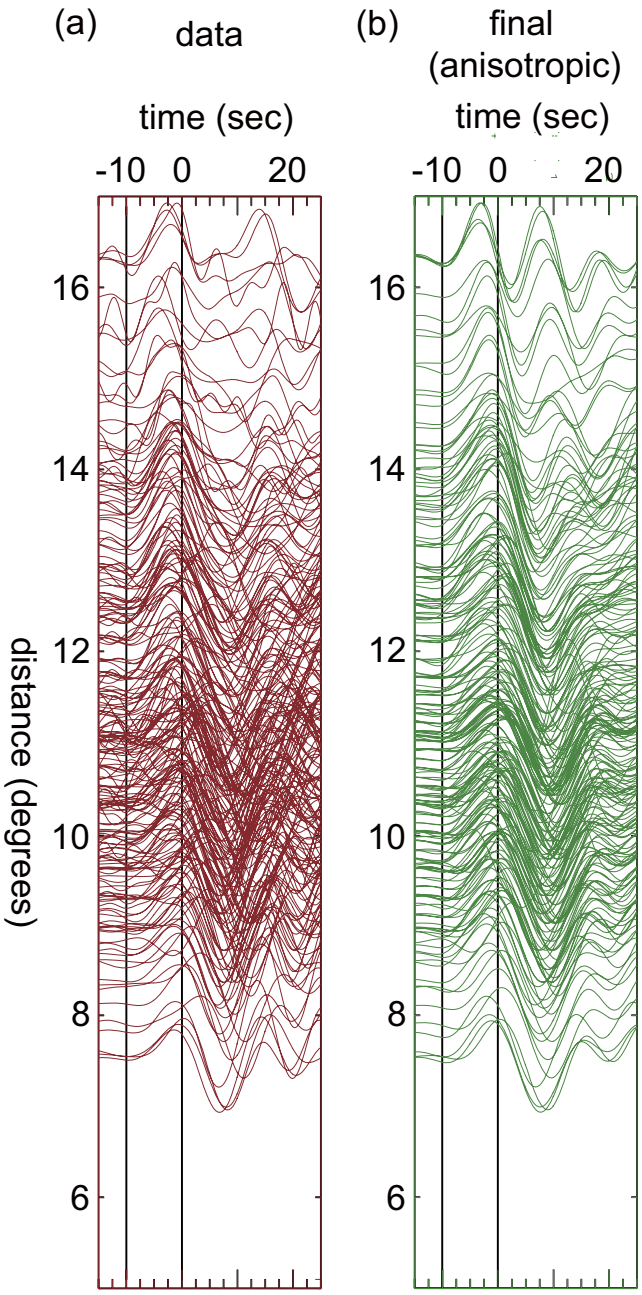

Figure S3. (a) Observed waveforms of Data Bin 1 (defined in Fig. S2). Anomalous data (the red lines in Fig. S2) are excluded. Source depth corrections to the seafloor surface were applied. (b) Synthetic waveforms for the final anisotropic model.

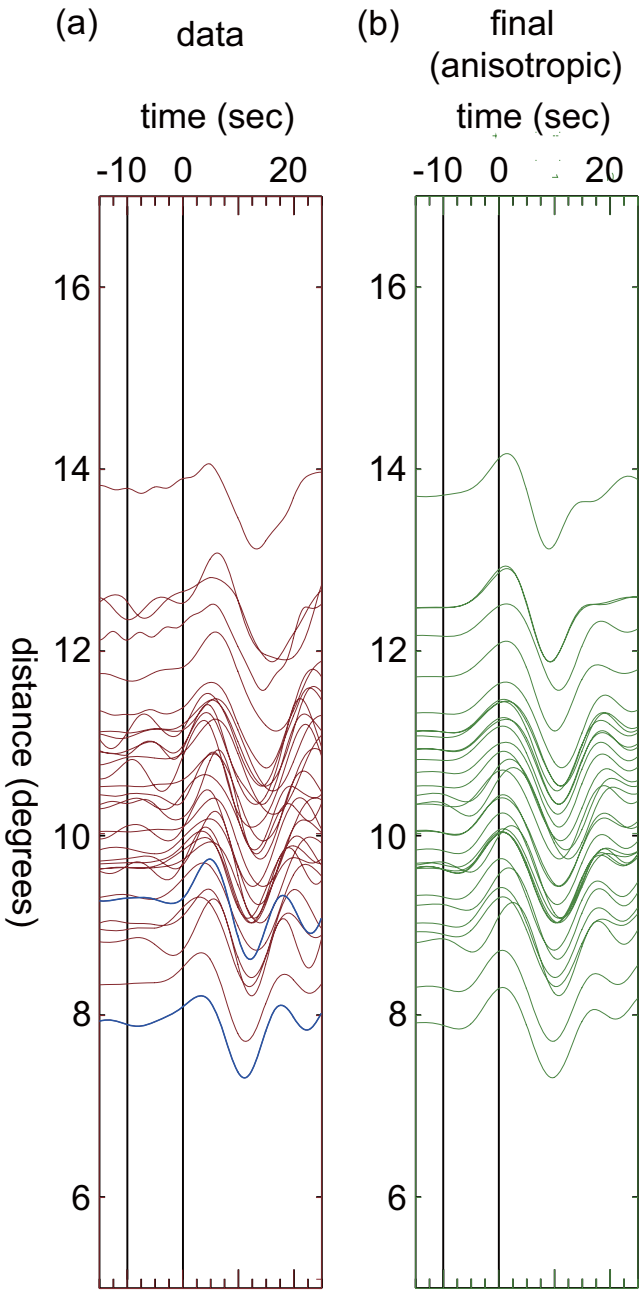

Figure S4. (a) Anomalous data (the red lines in Fig. S2) among the observed waveforms of Data Bin 1 (defined in Fig. S2). The waveforms discussed in the main text are denoted by the blue lines. (b) Synthetic waveforms for the final anisotropic model. Source depth corrections to the seafloor surface were applied.

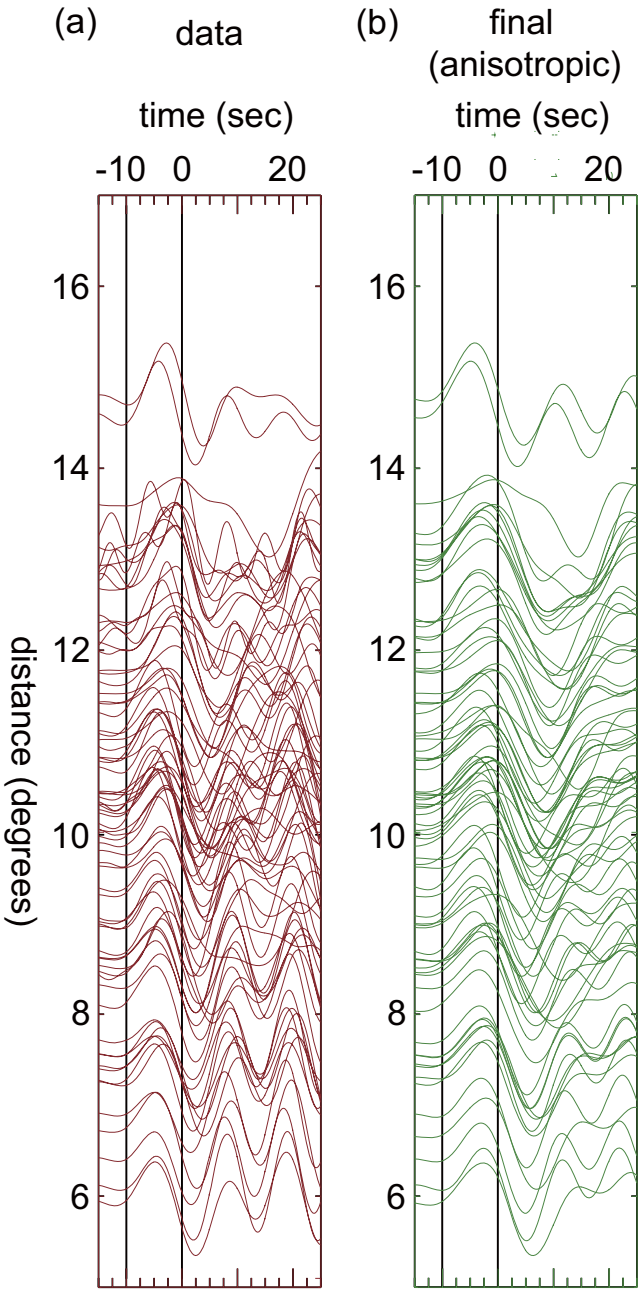

Figure S5. (a) Observed waveforms of Data Bin 2 (defined in Fig. S2). Waveforms observed in Area-A (see Fig. 1) are shown. (b) Synthetic waveforms for the final anisotropic model. Source depth corrections to the seafloor surface were applied.

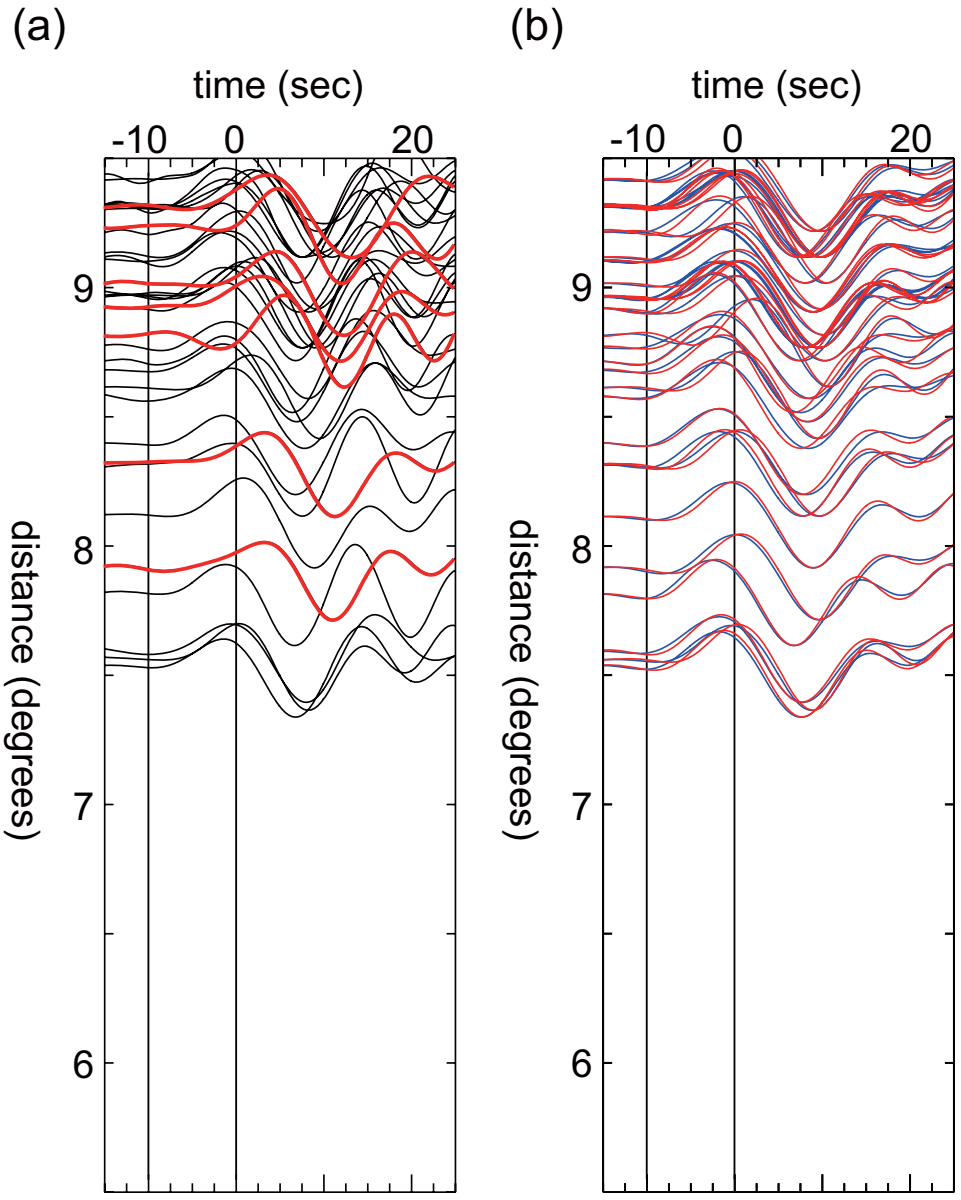

Figure S6. (a) Observed waveforms of Data Bin 1 (defined in Fig. S2) for closer distances. Anomalous data (the red lines in Fig. S2) are denoted by the thick red lines. (b) Synthetic waveforms for the final anisotropic model (red) and the final isotropic model (blue). Source depth corrections to the seafloor surface were applied.

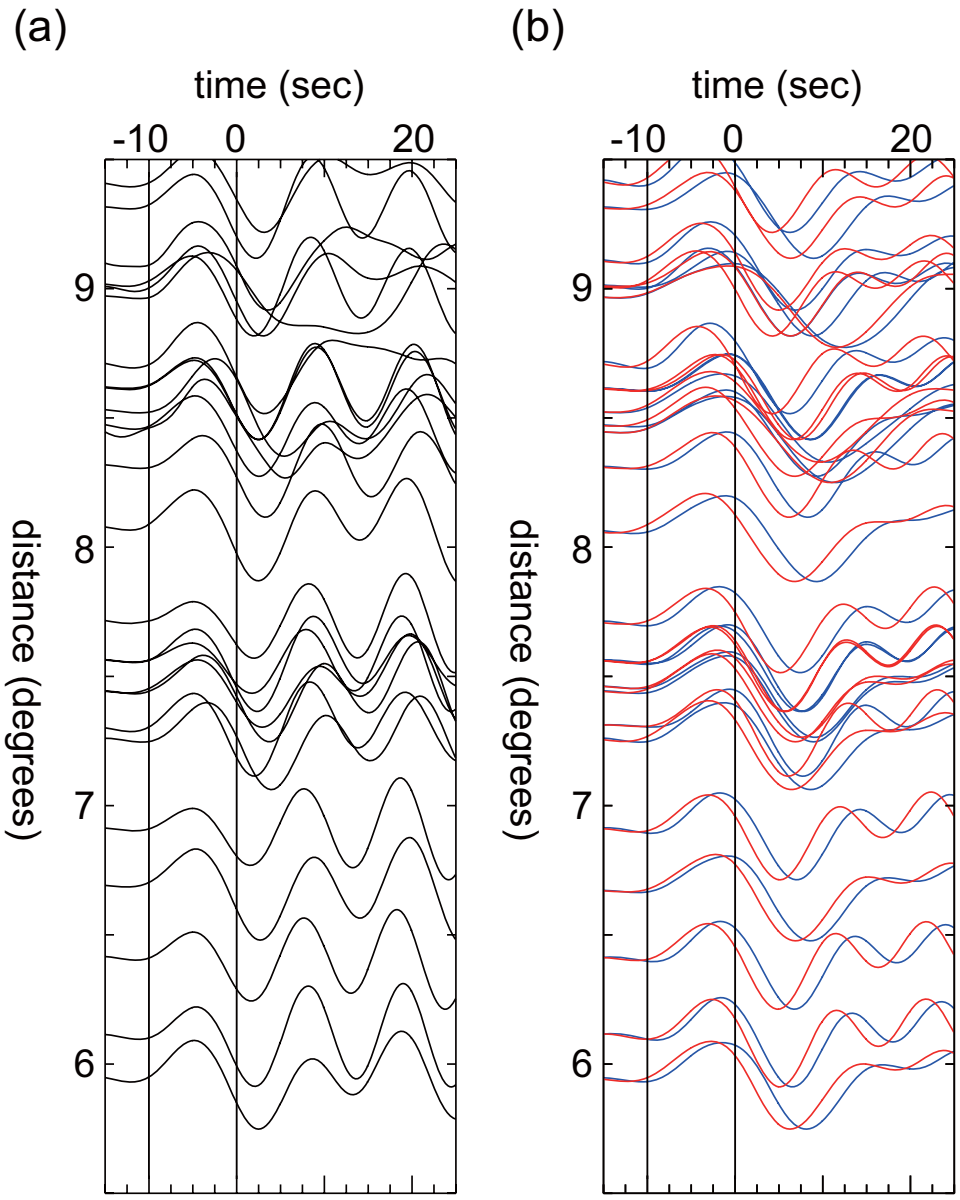

Figure S7. (a) Observed waveforms of Data Bin 2 (defined in Fig. S2) for closer distances. (b) Synthetic waveforms for the final anisotropic model (red) and the final isotropic model (blue). Source depth corrections to the seafloor surface were applied.

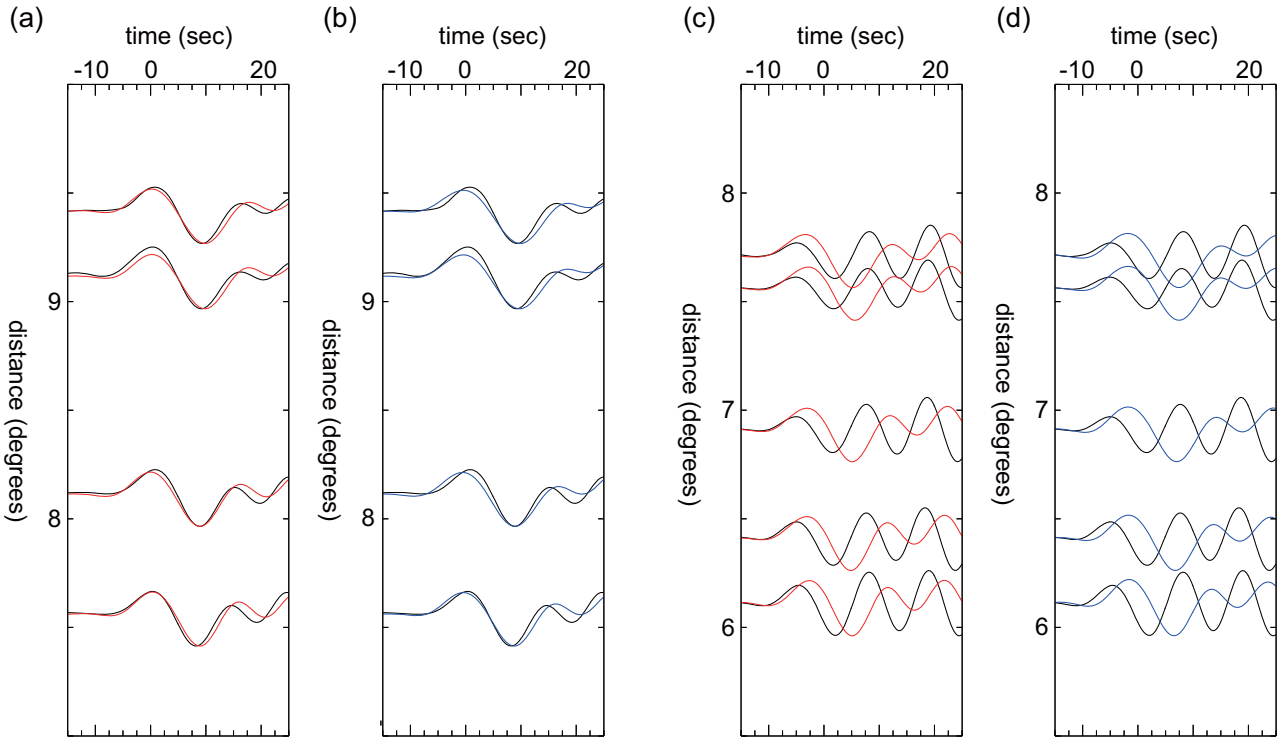

Figure S8. (a) Comparison of the observed waveforms (black) and synthetic seismograms for the final anisotropic model (red) for the event in Data Bin 1 (the event at 14:58:22.86, 05/05/2011). (b) The same as (a) but for the synthetic seismograms for the final isotropic model (blue). (c) Comparison of the observed waveforms (black) and synthetic seismograms for the final anisotropic model (red) for the event in Data Bin 2 (the event at 17:39:46.54, 09/08/2010). (d) The same as (c) but for the synthetic seismograms for the final isotropic model (blue). Source depth corrections to the seafloor surface were applied.

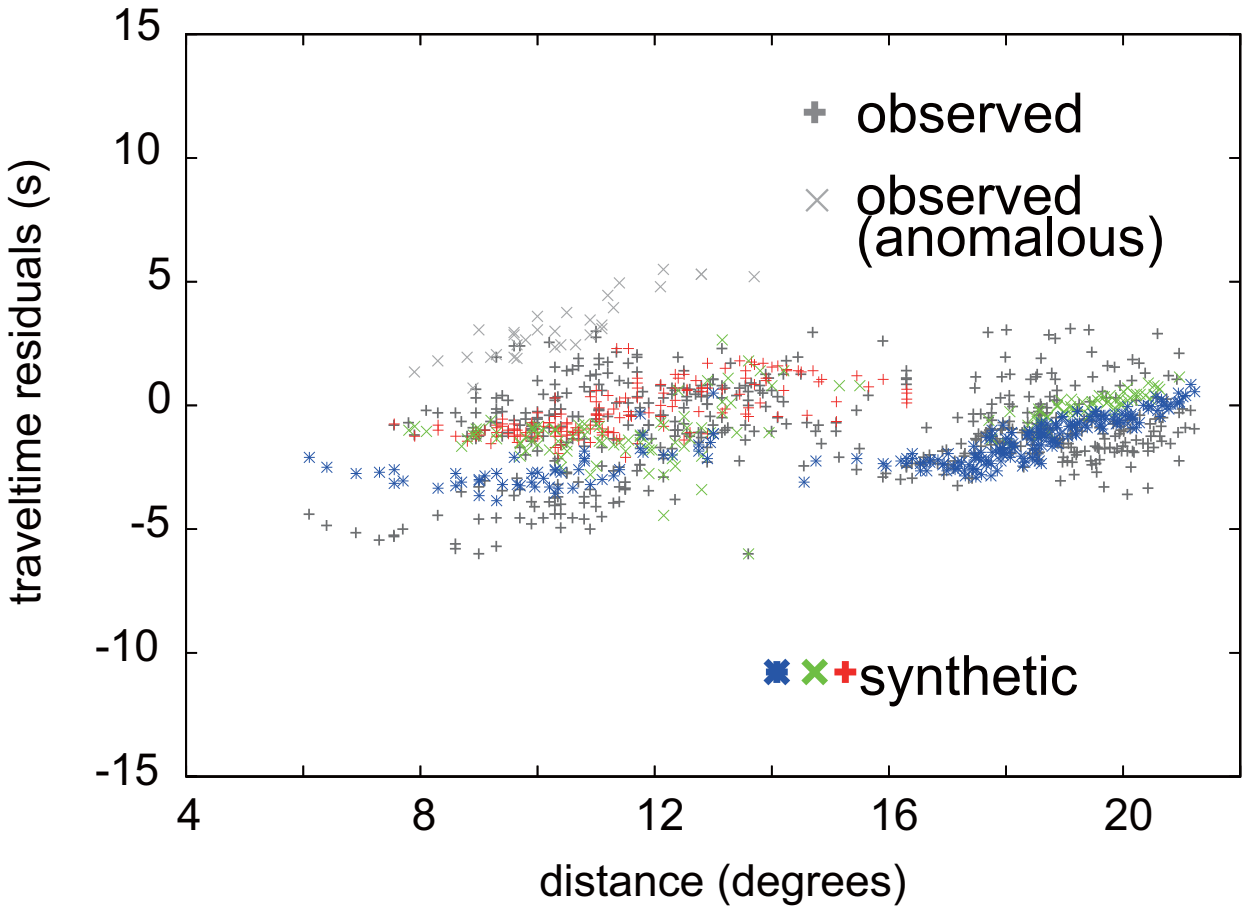

Figure S9. Comparison of the traveltime residuals measured for the observed waveforms (gray) and for the synthetic waveforms computed for the final isotropic model (green). The anomalous waveforms shown in Fig. S4 are denoted by the light gray crosses. Source depth corrections to the seafloor surface were applied.

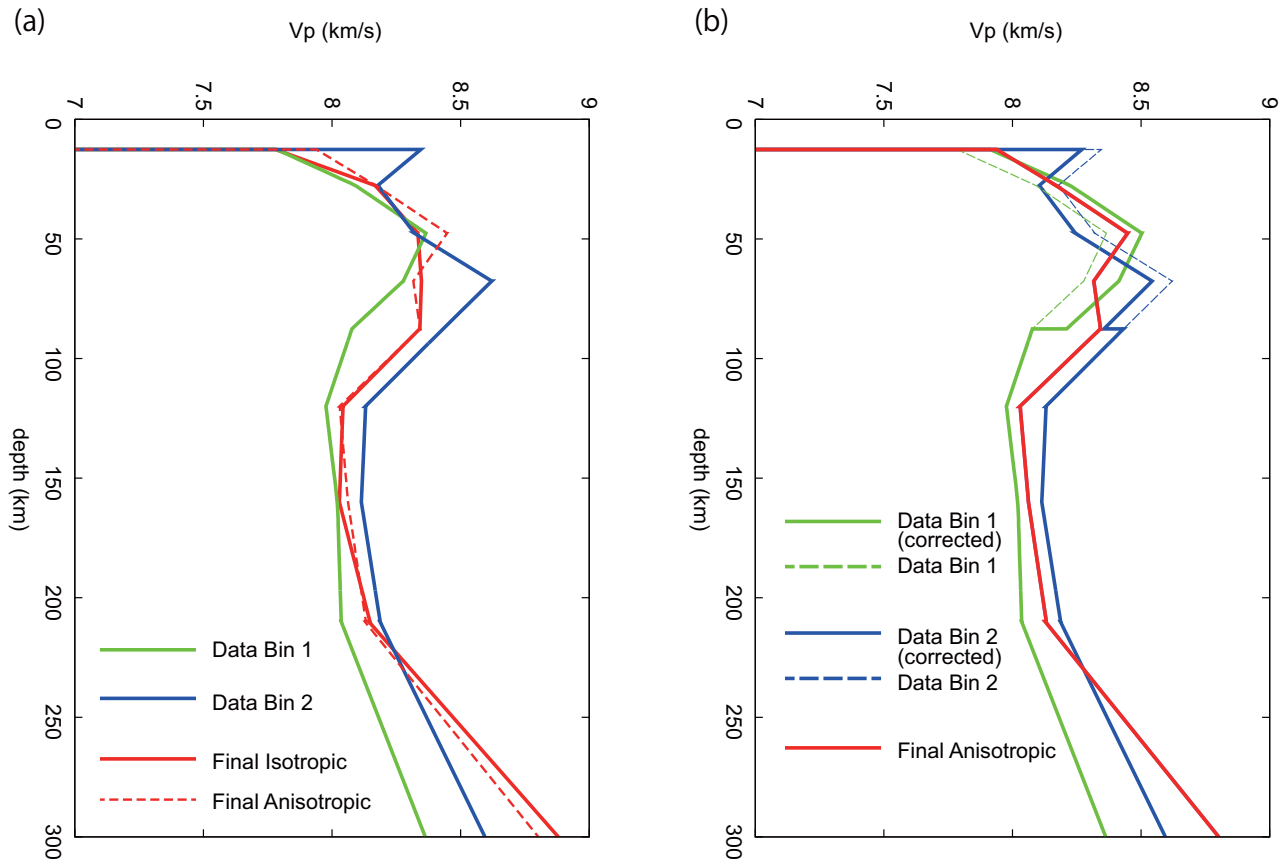

Figure S10. (a) Obtained models for Data Bin 1 (green) and Data Bin 2 (blue). The final isotropic model (red) and the final anisotropic model (dotted red) are also plotted. (b) Models for Data Bin 1 (green) and Data Bin 2 (blue) after the corrections of the lithospheric anisotropy. The final anisotropic model (red) is also plotted.

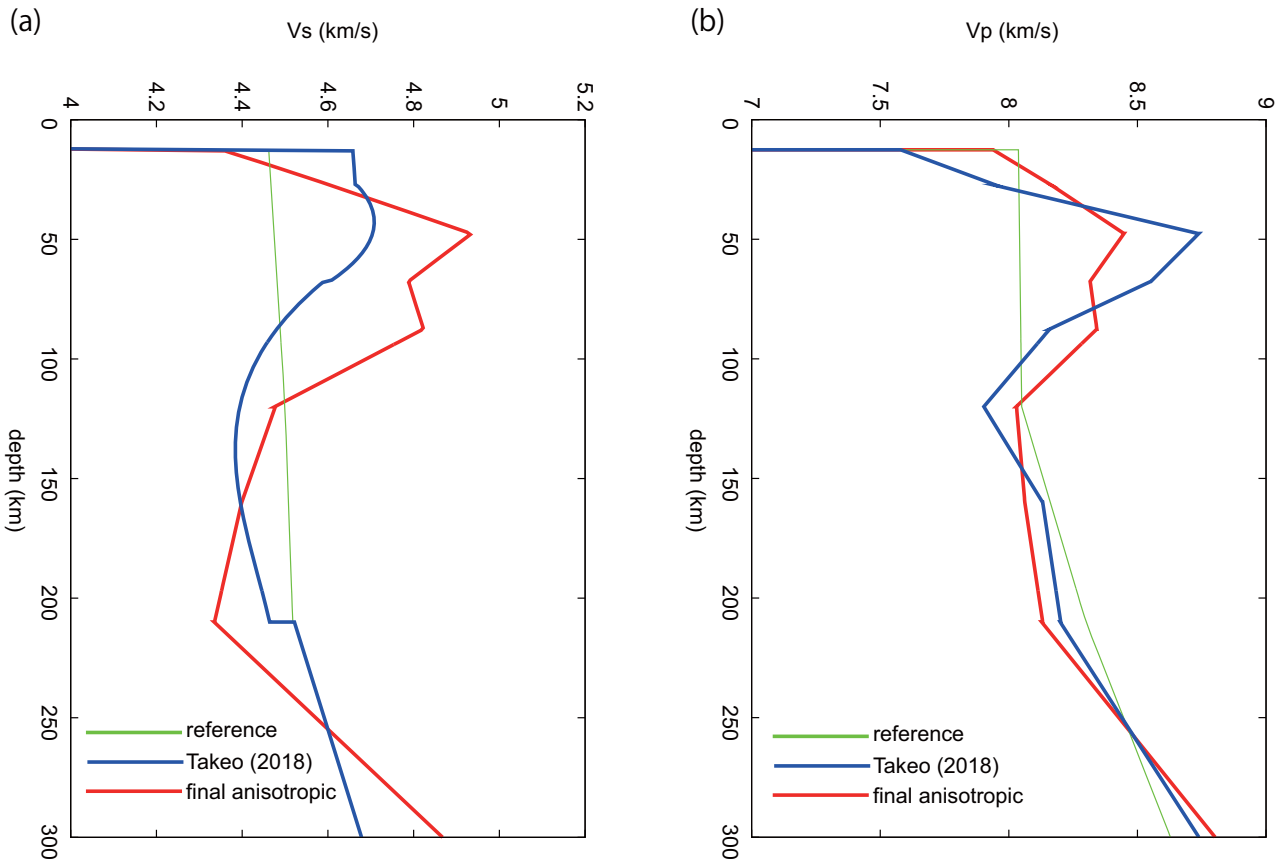

Figure S11. (a) Comparison of the V_S structures of the reference model (green), the final anisotropic model (red), and the model obtained by replacing the top 210 km structure of the reference model with the Area-A model of *Takeo et al.* [2018] (blue). (b) Comparison of the V_P structures between the final anisotropic model (red) and the model obtained by fixing the V_S structure to the model denoted by the blue line in (a) (blue). The reference model (green) is also plotted.

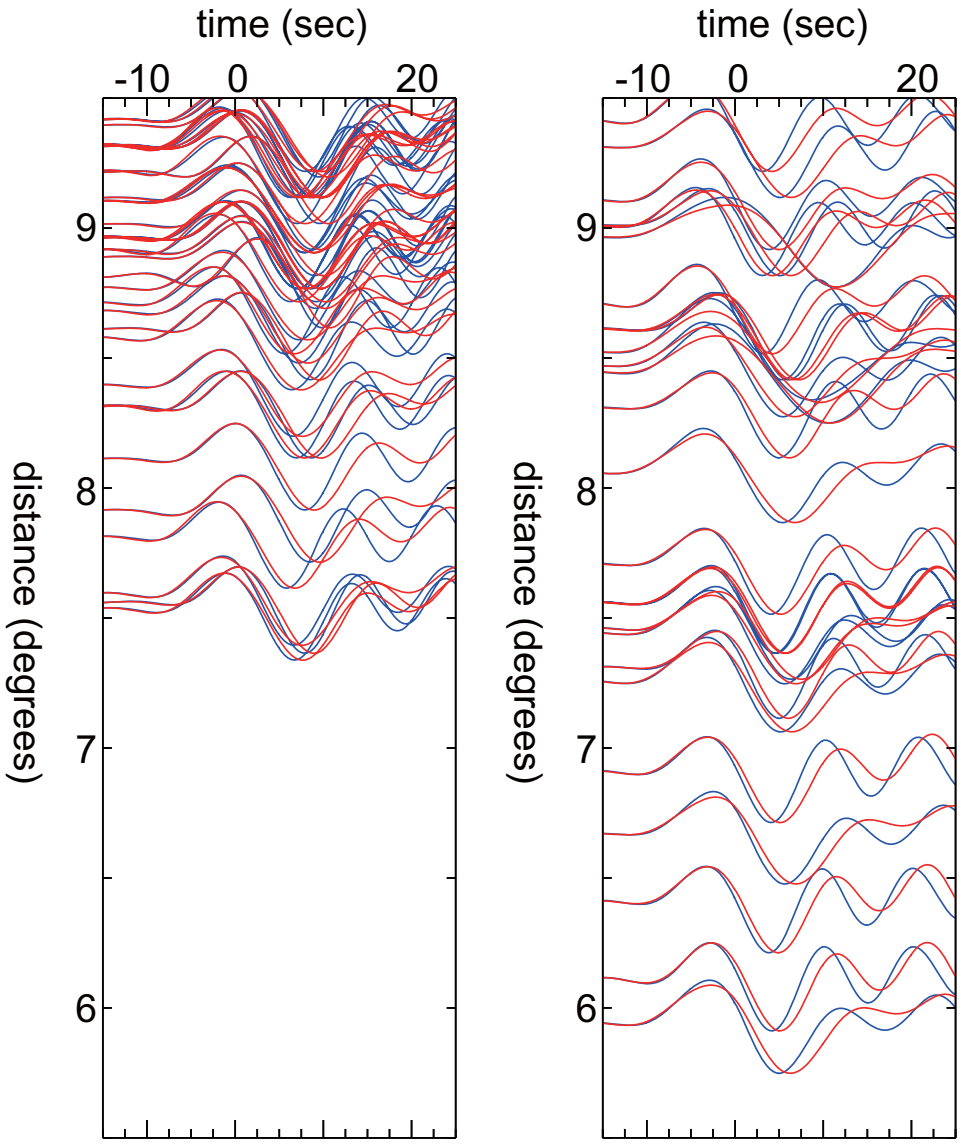

Figure S12. Synthetic record sections corresponding to Fig. S6 and Fig. S7. Synthetic seismograms for the final anisotropic model (red) and the final anisotropic model obtained by replacing the V_S structure with the model denoted by the blue line in Fig. S11a (blue) are shown. Source depth corrections to the seafloor surface were applied.

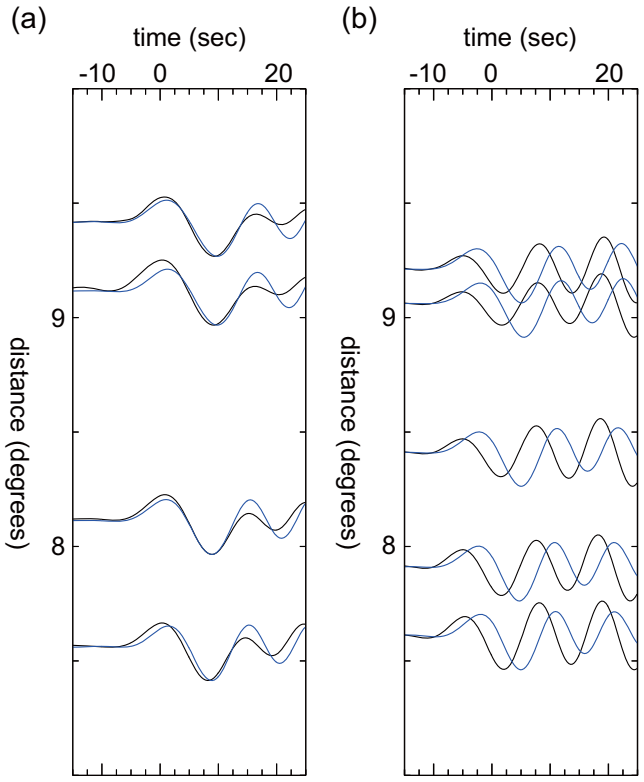

Figure S13. (a) Comparison of the observed waveforms (black) and synthetic seismograms computed for the model obtained by the test inversion (see the main text) whose V_P model and V_S model are denoted by the blue lines in Fig. S11b and S11a, respectively (blue). Comparison for the same event as in Fig. S8a is shown. (b) The same as (a) except that the comparison is for the event shown in Fig. S8c. Source depth corrections to the seafloor surface were applied.

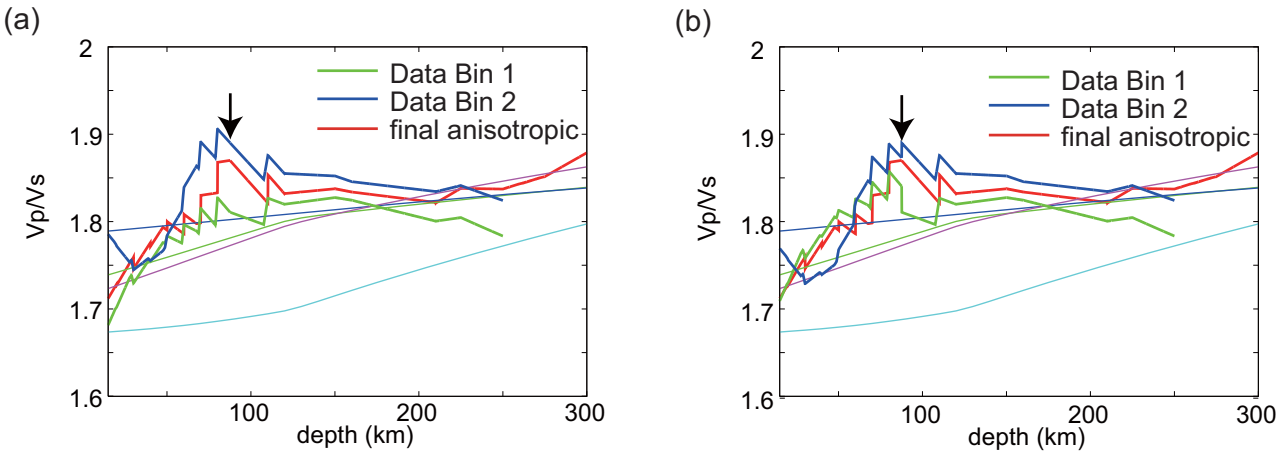

Figure S14. (a) The V_P/V_S models obtained by using the models in Fig. S10a. The model obtained by using the final anisotropic model is also plotted. (b) The same as (a) except for using the models in Fig. S10b.

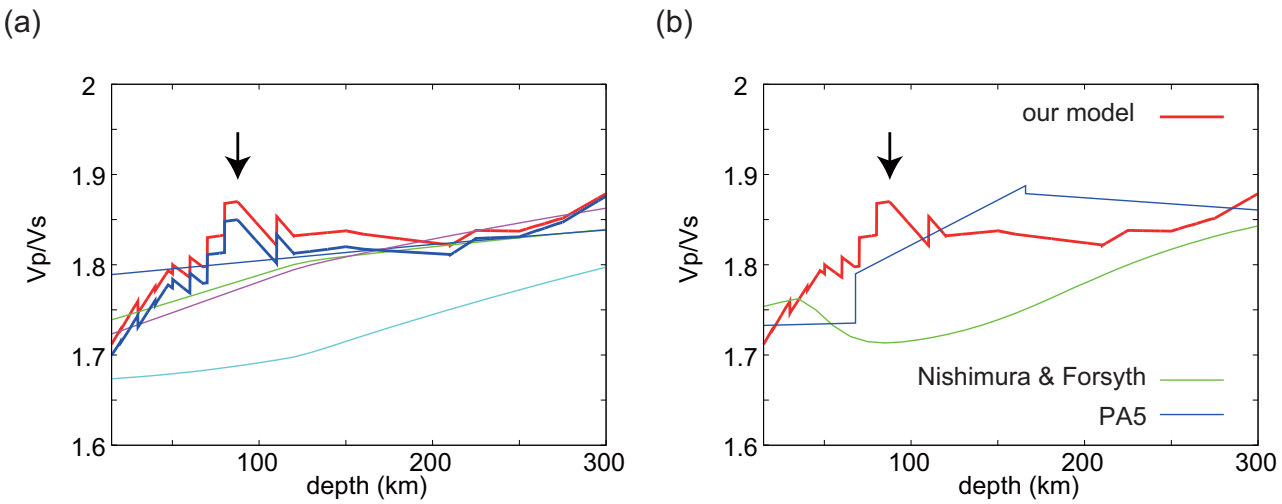

Figure S15. (a) The V_P/V_S model after the correction of the radial anisotropy (blue). The model before the correction (red) is also plotted. (b) The V_P/V_S values computed from the model by Nishimura and Forsyth [1989] (the model for > 110 Ma) and Gaherty and Jordan [1996] (the PA5 model). Our V_P/V_S model (red) is also plotted.

Table S1. Explicit V_P values (in km/s) of the final anisotropic models and the upper and lower bounds of the 2σ error presented in Fig. 8.

depth (km)	model	lower bound	upper bound
0.0	1.450	-	-
5.6	1.450	-	-
5.6	1.600	-	-
6.0	1.600	-	-
6.0	4.600	-	-
6.4	5.300	-	-
7.4	6.500	-	-
7.4	6.800	-	-
12.6	7.000	-	-
12.6	7.939	7.773	8.113
27.6	8.169	8.098	8.249
47.6	8.448	8.353	8.500
67.6	8.316	8.223	8.440
87.6	8.342	8.270	8.414
120.0	8.029	7.982	8.076
160.0	8.062	8.034	8.094
210.0	8.130	8.097	8.179
310.0	8.880	8.796	8.932
410.0	8.725	8.632	8.820
410.0	9.038	8.938	9.139
660.0	10.109	9.983	10.262